Heat Transfer in the Flow of a Cold, Axisymmetric Vertical Liquid Jet Against a Hot, Horizontal Plate

Jian-Jun Shu[1]

Graham Wilks

School of Mechanical and Aerospace
Engineering,
Nanyang Technological University,
50 Nanyang Avenue,
Singapore 639798, Singapore

The paper considers heat transfer characteristics of thin film flow over a hot horizontal flat plate resulting from a cold vertical jet of liquid falling onto the surface. A numerical solution of high accuracy is obtained for large Reynolds numbers using the modified Keller box method. For the flat plate, solutions for axisymmetric jets are obtained. In a parallel approximation theory, an advanced polynomial approximation for the velocity and temperature distribution is employed and results are in good agreement with those obtained using a simple Pohlhausen polynomial and the numerical solutions.
[DOI: 10.1115/1.2780180]

1 Introduction

As has been noted earlier, the draining flow of liquid under gravity through banks of horizontal tubes occurs frequently in technological processes involving heat or mass transfer. The mode of drainage may be in the form of droplets, columns, or continuous sheets. After having examined the sheet mode of drainage, it is natural to move on to a closer inspection of the columnar mode of drainage. Again, if the film thickness is small relative to a typical tube dimension, the impact surface may be regarded as locally plane [1]. Accordingly, an initial prototype model for columnar impingement is simply that of a vertical round jet striking a plane horizontal surface. The flow model is thus axisymmetric, and considerable simplification of the governing equations can be made. Some detailed understanding of the flow and heat transfer characteristics at the point of impingement may be obtained and possible methodologies identified for examining the nonaxisymmetric flow in due course.

Analytically, Watson [2] found a similarity solution of the boundary-layer equations governing such a flow and also considered by approximate methods the initial growth of the boundary layer from the stagnation point where the similarity solution does not hold. Chaudhury [3] obtained a supplementary thermal solution using an orthogonal polynomial. Some recent progress [1,4–9] has been made in investigating various problems of a liquid jet impinging on a solid surface. In this paper, the theoretical results are improved and an accurate numerical solution is obtained for the heat transfer in the flow of a cold, axisymmetric vertical liquid jet against a hot horizontal plate.

2 Modeling

The problem to be examined concerns film cooling, which occurs when a cold vertically draining column strikes a hot horizontal plate. Although a column of fluid draining under gravity is accelerated and thin at impact [10,11], it is reasonable to model the associated volume flow as a jet of uniform velocity U_0 and radius H_0, as illustrated in Fig. 1(a). The notation $Q = \pi H_0^2 U_0$ is

introduced for the flow rate and a film Reynolds number may be defined as $\mathrm{Re} = U_0 H_0 / \nu$, where ν is the kinematic viscosity of the fluid. The underlying hydrodynamics of the fluid flow have been delineated by Watson [2]. Exactly the same physical assessment of the flow field applies, as was outlined in Ref. [4]. Subregions (i)–(v) are once again appropriate and the solution, to follow, similarly uses this understanding of the basic hydrodynamics.

In practice, the flow against a plane wall is terminated by a hydraulic jump. The objective here is in due course to develop a methodology for the flow around a tube where no such phenomenon is observed. Accordingly, the associated complications of a possible hydraulic jump will not be considered.

Heat transfer estimates can be obtained under the assumptions of a constant temperature T_w at the plane and zero heat flux on the free surface. When water is the coolant medium, then it has to be noted that the rates of viscous and thermal diffusion are appreciably different, and the point at which viscous effects penetrate the free surface occurs before the point at which the free surface first experiences the presence of the hot plane. To develop an approximation, the flow field is thus divided into regions, as illustrated in Fig. 1(b).

2.1 Region 1. When an impinging circular jet strikes a plane surface, it experiences an eventually inviscid radially symmetric division and deflection through 90 deg. In the immediate vicinity of the point of impact, viscous effects begin to influence the flow field. At that point, an imbedded axisymmetric stagnation boundary layer of thickness $O(\nu H_0 / U_0)^{1/2}$ or $O(H_0 \mathrm{Re}^{-1/2})$ occurs. For high flow rates $\mathrm{Re} \gg 1$ and to a first approximation, the stagnation boundary-layer thickness is negligibly small. The presence of the solid boundary more significantly influences the flow within the deflected jet away from the point of impact. Here, a viscous boundary layer develops against the horizontal plate. The effects of viscosity are eventually present throughout the film and the form of a solution identifies a point of viscous penetration of the free surface, marking the end of Region 1. For Prandtl numbers greater than 1, a parallel thermal diffusion occurs, but thermal effects do not penetrate the free surface at the end of Region 1.

2.2 Region 2. Over Region 2, thermal diffusion continues until the presence of the hot plate eventually influences the free surface. This point of penetration marks the end of Region 2. Accordingly, Region 2 describes the developing temperature distribution within an established hydrodynamic flow field since the
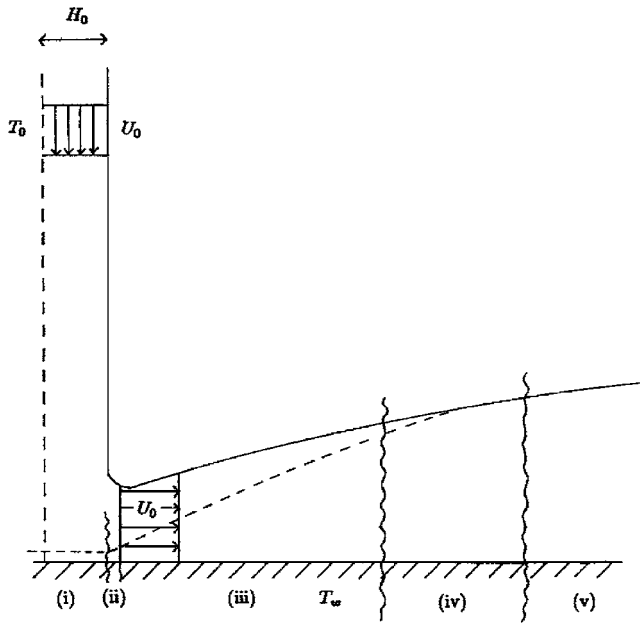
(i) Imbedded stagnation boundary layer
(ii) Outer inviscid deflection region
(iii) Quasi Blasius viscous diffusion
(iv) Transition around viscous penetration
(v) Similarity film flow
The dashed line represents the hydrodynamic boundary layer.

(a)
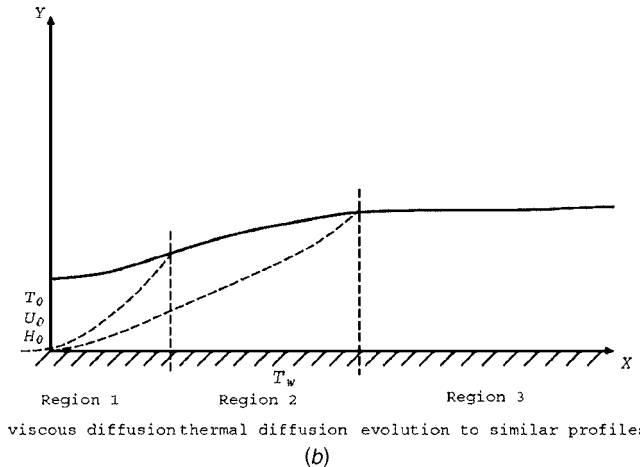
viscous diffusion thermal diffusion evolution to similar profiles

(b)

Fig. 1 (*a*) **The vertical jet and resultant film for the axisymmetric flat plate. (i) imbedded stagnation boundary layer, (ii) outer inviscid deflection region, (iii) quasi-Blasius viscous diffusion, (iv) transition around viscous penetration, and (v) similarity film flow. The dashed line represents the hydrodynamic boundary layer. (*b*) Basis of approximate solution.**

form of the solution in Region 1 is designed to coalesce directly with the Watson similarity solution for velocity and film thickness at the boundary between Regions 1 and 2.

2.3 Region 3. Once the influence of the hot plate penetrates the free surface, the surrounding air acts as an insulator, and here, there is zero heat flux from the free surface. As a consequence, the film gradually approaches a uniform temperature distribution, coinciding with the temperature of the plate. Region 3 monitors the approach to this asymptotic state.

To assess the validity of the approximate method, a full numerical solution of the model equations is then obtained. Results and comparisons are presented at the conclusion of the paper.

3 Governing Equations

The flow under investigation has been modeled as a steady, axisymmetric flow of incompressible fluid. In the absence of body forces and viscous dissipation, the equations expressing conservation of mass, momentum, and energy are, consequently,

$$\nabla \cdot V = 0 \tag{1}$$

$$\rho(V \cdot \nabla)V = -\nabla P + \mu \nabla^2 V \tag{2}$$

$$\rho C_p(V \cdot \nabla)T = k\nabla^2 T \tag{3}$$

where $\mathbf{V} = (v_r, v_z)$ are velocity components associated with cylindrical coordinates (r, z) measured along the plate from the axis of deflection and normal to the plate, respectively. ρ, μ, C_p, and k are the density, dynamic viscosity, specific heat at constant pressure, and thermal conductivity of the cooling fluid in the jet, respectively. T and P are, respectively, the temperature and pressure within the fluid.

The specific boundary conditions under which the equations are to be solved closely parallel those of Ref. [4]. In particular, at the wall, the no slip condition and the constant temperature T_w require

$$v_r = v_z = 0 \; T = T_w \quad \text{at } z = 0, \; r \geqslant 0 \tag{4}$$

On the free surface, assuming negligible shear stress and heat flux requires

$$\frac{\partial v_r}{\partial z} = 0 \quad \frac{\partial T}{\partial z} = 0 \quad \text{at } z = H(r), \; r \geqslant 0 \tag{5}$$

The conservation of volume constraint applies at any given r station and, hence,

$$2\pi \int_0^{H(r)} r v_r(r,z) dz = \text{const} = \pi H_0^2 U_0 \quad \text{for } r \geqslant 0 \tag{6}$$

Under the assumption that the film thickness remains thin relative to a characteristic horizontal dimension, a boundary-layer treatment of the equations leads to a significant simplification.

The following nondimensional variables are introduced:

$$x = \frac{r}{\text{Re}^{1/3} H_0}, \quad \bar{Y} = \frac{\text{Re}^{1/3} z}{H_0} \tag{7}$$

$$\bar{H}(x) = \frac{\text{Re}^{1/3} H(r)}{H_0} \tag{8}$$

$$\bar{U} = \frac{v_r}{U_0}, \quad \bar{V} = \frac{\text{Re}^{2/3} v_z}{U_0}, \quad \bar{\phi} = \frac{T - T_w}{T_0 - T_w}, \quad p = \frac{P}{\rho U_0^2} \tag{9}$$

In the limit $\text{Re} \to +\infty$ with x remaining $O(1)$, the following equations are obtained:

$$\frac{\partial}{\partial x}(x\bar{U}) + \frac{\partial}{\partial \bar{Y}}(x\bar{V}) = 0 \tag{10}$$

$$\bar{U}\frac{\partial \bar{U}}{\partial x} + \bar{V}\frac{\partial \bar{U}}{\partial \bar{Y}} = -\frac{\partial p}{\partial x} + \frac{\partial^2 \bar{U}}{\partial \bar{Y}^2} \tag{11}$$

$$0 = \frac{\partial p}{\partial \bar{Y}} \tag{12}$$

$$\text{Pr}\left(\bar{U}\frac{\partial \bar{\phi}}{\partial x} + \bar{V}\frac{\partial \bar{\phi}}{\partial \bar{Y}}\right) = \frac{\partial^2 \bar{\phi}}{\partial \bar{Y}^2} \tag{13}$$

where $\text{Pr} = \nu/\kappa$ is the Prandtl number with ν as the kinematic viscosity, μ/ρ, and κ as the thermometric conductivity, $k/\rho C_p$ and $\Delta T = T_w - T_0$. In common with standard boundary-layer theory, Eq.

(12) implies that the pressure across the film remains constant. In the absence of external pressure gradients and with zero shear assumed on the free surface, the pressure term in Eq. (11) is identically zero.

In nondimensional variables, the boundary conditions now read

$$\bar{U} = \bar{V} = \bar{\phi} = 0 \quad \text{at } \bar{Y} = 0, \ x \geq 0 \tag{14}$$

$$\frac{\partial \bar{U}}{\partial \bar{Y}} = \frac{\partial \bar{\phi}}{\partial \bar{Y}} = 0 \quad \text{at } \bar{Y} = \bar{H}(x), \ x \geq 0 \tag{15}$$

$$\int_0^{\bar{H}(x)} x \bar{U} d\bar{Y} = \frac{1}{2} \quad \text{for } x \geq 0 \tag{16}$$

These have been quoted in the context of the fully developed film flow field, which is approached in Region 3. The hydrodynamic equations of this system have been shown by Watson [2] to possess similarity solutions. A simple supplementary thermal solution of uniform temperature is also present. These solutions provide the basis for developing comprehensive approximations for the complete flow field downstream of the radial symmetry point of impingement incorporating Regions 1–3.

4 Downstream Similarity Solutions

The equations to be solved are

$$\frac{\partial}{\partial x}(x\bar{U}) + \frac{\partial}{\partial \bar{Y}}(x\bar{V}) = 0 \tag{17}$$

$$\bar{U}\frac{\partial \bar{U}}{\partial x} + \bar{V}\frac{\partial \bar{U}}{\partial \bar{Y}} = \frac{\partial^2 \bar{U}}{\partial \bar{Y}^2} \tag{18}$$

$$\Pr\left(\bar{U}\frac{\partial \bar{\phi}}{\partial x} + \bar{V}\frac{\partial \bar{\phi}}{\partial \bar{Y}}\right) = \frac{\partial^2 \bar{\phi}}{\partial \bar{Y}^2} \tag{19}$$

subject to boundary conditions (14)–(16).

Note that the equations governing the hydrodynamics (Eqs. (17) and (18)) are independent of the energy equation (Eq. (19)). These are examined as follows. It is well known that, using Mangler's transformations [12], the calculation of axially symmetrical boundary layers on bodies of revolution, in an unlimited expanse of fluid, can be reduced to the calculation of complementary two-dimensional flows. The flow currently under consideration represents the axially symmetric equivalent of the two-dimensional flow examined in Ref. [4]. Here, we examine the possibility that the Mangler's transformations applied to the set of Eqs. (17) and (18) under the specified hydrodynamic boundary conditions have a two-dimensional equivalent differential system.

Let

$$x' = \int_0^x t^2 dt = \frac{x^3}{3} \tag{20}$$

and

$$\bar{Y}' = x\bar{Y} \tag{21}$$

then

$$\bar{U}' = \bar{U} \tag{22}$$

$$\bar{V}' = \frac{1}{x}\left(\bar{V} + \frac{\bar{Y}\bar{U}}{x}\right) \tag{23}$$

With these new' variables, Eqs. (17) and (18) become

$$\frac{\partial \bar{U}'}{\partial x'} + \frac{\partial \bar{V}'}{\partial \bar{Y}'} = 0 \tag{24}$$

$$\bar{U}'\frac{\partial \bar{U}'}{\partial x'} + \bar{V}'\frac{\partial \bar{U}'}{\partial \bar{Y}'} = \frac{\partial^2 \bar{U}'}{\partial \bar{Y}'^2} \tag{25}$$

The boundary conditions are

$$\bar{U}' = \bar{V}' = 0 \quad \text{at } \bar{Y}' = 0 \tag{26}$$

$$\frac{\partial \bar{U}'}{\partial \bar{Y}'} = 0 \quad \text{at } \bar{Y}' = x\bar{H}(x) = \bar{H}'(x') \tag{27}$$

and

$$\int_0^{\bar{H}'(x')} \bar{U}' d\bar{Y}' = \frac{1}{2} \tag{28}$$

With the minor modification of the conservation of volume flow constraint, the differential system formally reproduces the hydrodynamic system examined in Ref. [4]. Introducing a similarity variable $\eta = \bar{Y}'/\bar{H}'(x')$, a stream function form of solution $\psi(x, \bar{Y}') = \bar{U}_s(x)\bar{h}(x)f(\eta)$ leads to the Watson similarity solution as the solution of

$$2f''' + 3c^2 f'^2 = 0 \quad f'(0) = 0 \quad f'(1) = 1 \quad f''(1) = 0$$

Here, $\bar{U}_s(x)$ represents the nondimensional unknown velocity at the free surface and c can be obtained analytically as

$$\frac{\Gamma(1/3)\Gamma(1/2)}{3\Gamma(5/6)} \approx 1.402$$

As a result, the axisymmetric solution can be directly inferred from the solution of Ref. [4] as

$$\bar{U}_s(x) = \frac{27c^2}{8\pi^2(x^3 + l^3)} \tag{29}$$

$$\bar{h}(x) = \frac{2\pi}{3\sqrt{3}}(x^3 + l^3) \tag{30}$$

Here, l is a nondimensional leading edge shift constant. The solutions hold at large distances from the jet incidence and l may be associated with an indeterminate origin of such a flow solution. An estimate of l may be obtained by further consideration of the growth of the boundary layer from the point of impact of the jet. The effects of viscous retardation are seen to result in a simultaneous thickening of the film and a reduction in the free surface velocity.

In the original dimensional variables,

$$U_s(r) = \frac{27c^2}{8\pi^4}\frac{Q^2}{\nu(r^3 + L^3)} \tag{31}$$

$$H(r) = \frac{2\pi^2}{3\sqrt{3}}\frac{\nu}{Q}\frac{(r^3 + L^3)}{r} \tag{32}$$

The velocity distribution within the film is given by

$$v_r(r,z) = U_s(r)f'(\eta) \tag{33}$$

where $f(\eta)$ is the Watson similarity solution whose properties have been presented in Ref. [4].

The associated asymptotic downstream similarity solution for the temperature distribution is obtained by examining Eq. (19) with $\bar{\phi}(x, \bar{Y}) = \bar{\phi}(\eta)$, together with the associated similarity transformations. The resultant equation is

$$\bar{\phi}'' = 0 \tag{34}$$

subject to the boundary conditions

$$\bar{\phi}(0) = 0 \quad \bar{\phi}'(1) = 0 \qquad (35)$$

The solution must therefore be $\bar{\phi} \equiv 0$, confirming a uniform temperature distribution in the film equal to the temperature of the plate, T_w.

5 Approximate Solutions

The solutions obtained in the previous section are asymptotic solutions, which are valid well downstream of the location of jet impingement and deflection along the plane. An approximation scheme is now presented, which looks more closely at the flow at impingement. The solution is built up from this vicinity, stage by stage, to provide comprehensive details of the velocity and temperature distribution at radial stations away from the origin.

5.1 Region 1. The discussion of Region 1 follows closely that of the sheet drainage flow of Ref. [4]. At impact, an inviscid deflection of the draining sheet occurs over a negligibly small length scale. Only after deflection is the flow aware of the presence of the solid boundary, and only then do viscous effects begin to influence the flow field. The development of a viscous boundary layer within a uniform velocity film accounts for the close parallel in this region with Blasius boundary-layer flow. Similarly, the temperature differential between the plane and the fluid only begins to influence the temperature distribution after deflection. Thus, a developing thermal boundary layer may also be anticipated from $r=0$.

The equations governing the viscous and thermal boundary layers are exactly the same as Eqs. (17)–(19), but the boundary conditions, as in Ref. [4], now read

$$\bar{U} = 0, \quad \bar{V} = 0, \quad \bar{\phi} = 0 \quad \text{at } \bar{Y} = 0, \, x \geq 0$$

($\bar{U} \to 1$, $\phi \to 1$ as $\bar{Y}$ approaches the outer limits of the viscous and thermal boundary layers, respectively)

$$\bar{U} = 1, \quad \bar{\phi} = 1 \quad \text{at } x = 0, \, \bar{Y} > 0$$

The transformations

$$\psi(x, \bar{Y}) = \sqrt{\frac{2}{3}} x^{3/2} \bar{f}(\bar{\eta}), \quad \bar{\phi}(x, \bar{Y}) = \bar{\phi}(\bar{\eta}), \quad \bar{\eta} = \sqrt{\frac{3}{2}} \frac{\bar{Y}}{x^{1/2}}$$

$$\bar{U} = \frac{1}{x} \frac{\partial \psi}{\partial \bar{Y}}, \quad \bar{V} = -\frac{1}{x} \frac{\partial \psi}{\partial x} \qquad (36)$$

lead once again to

$$\bar{f}''' + \bar{f}\bar{f}'' = 0$$

$$\frac{1}{\Pr} \bar{\phi}'' + \bar{f}\bar{\phi}' = 0$$

subject to boundary conditions

$$\bar{f}(0) = 0, \quad \bar{f}'(0) = 0, \quad \bar{\phi}(0) = 0$$

$$\bar{f}'(\bar{\eta}) \to 1, \quad \bar{\phi}(\bar{\eta}) \to 1 \quad \text{as } \bar{\eta} \to +\infty$$

Full details of these solutions may be referred to in Ref. [4]. Following the arguments of Ref. [4], a device which essentially suppresses the transition region may be introduced. An approximate velocity profile,

$$\bar{U}(x, \bar{Y}) = \bar{U}_s(x) f'\left(\frac{\bar{Y}}{\delta}\right), \quad \eta = \frac{\bar{Y}}{\delta(x)} \qquad (37)$$

is assumed, where $f'(\eta)$ is the original Watson similarity profile and $\delta(x)$ is the nondimensional boundary-layer thickness. The profile is then used in a Kármán–Pohlhausen method of solution. Over Region 1, unretarded fluid is present when $x < x_0$, say, where x_0 marks the point of penetration of viscous effects on the free

surface, so that $\bar{U}_s(x) = 1$ and $\delta(x) < \bar{h}(x)$ over $0 < x < x_0$. For $x > x_0$ into Region 2, $\delta(x) \equiv \bar{h}(x)$ and $\bar{U}_s(x) < 1$ in a manner that, using the conservation of flow constraint, can be matched directly onto the asymptotic similarity solutions.

The use of $f'(\eta)$ is feasible only because its integral properties are readily available for use in the momentum integral equation, which reads

$$\left(\frac{1}{x^2}\right) \frac{d}{dx} \int_0^{\delta(x)} \bar{U}(1 - \bar{U}) d\bar{Y} = \left(\frac{\partial \bar{U}}{\partial \bar{Y}}\right)_{\bar{Y}=0} \qquad (38)$$

Using Eq. (37) gives

$$\left(\frac{1}{x^2}\right) \frac{d}{dx} \left\{ \delta(x) \int_0^1 f'(1 - f') d\eta \right\} = \frac{f''(0)}{\delta(x)} = \frac{c}{\delta(x)}$$

The integral

$$\int_0^1 (f' - f'^2) d\eta = \frac{2(\pi - c\sqrt{3})}{3\sqrt{3} c^2} \qquad (39)$$

and the equation for the boundary-layer thickness is

$$\frac{d}{dx}(\delta^2) = \frac{3\sqrt{3} c^3 x^2}{\pi - c\sqrt{3}}$$

and, hence,

$$\delta^2(x) = \frac{\sqrt{3} c^3 x^3}{\pi - c\sqrt{3}} \qquad (40)$$

where $\delta(x) = 0$ has been assumed at $x=0$, which is valid in the limit of the underlying assumption.

Invoking the conservation of volume flow at x_0, the end point of Region 1 effectively suppresses the transition region and leads to

$$\int_0^{\delta(x)} \bar{U} d\bar{Y} + (\bar{h} - \delta) = \frac{1}{2} \qquad (41)$$

or

$$\delta \int_0^1 f'(\eta) d\eta + (\bar{h} - \delta) = \frac{1}{2} \qquad (42)$$

giving

$$\bar{h}(x) = \frac{1}{2} + \left(1 - \frac{2\pi}{3\sqrt{3} c^2}\right) \delta \qquad (43)$$

Since $\delta(x_0) = \bar{h}$,

$$x_0 = \sqrt[3]{\frac{9\sqrt{3} c (\pi - c\sqrt{3})}{16\pi^2}} \approx 0.46216 \qquad (44)$$

and matching the free surface velocity at $x = x_0$ leads to

$$l = \sqrt[3]{\frac{9\sqrt{3} c}{16\pi^2}} (3\sqrt{3} c - \pi) \approx 0.8308 \qquad (45)$$

5.2 Alternative Profiles. The fact that the integral properties of the Watson similarity profile are readily calculated has been used to advantage in Sec. 5.1. Its use, however, in the energy integral equation is not as convenient as a polynomial representation or approximation for the velocity profile. For instance, the Pohlhausen profile

$$f_p'(\eta) = 2\eta - 2\eta^3 + \eta^4 \qquad (46)$$

may again be used in assessing aggregate properties of the flow.

The result is an estimate of the boundary-layer thickness given by

$$\delta_p^2 = \frac{420x^3}{37} \qquad (47)$$

which leads to

$$x_{0_p} = \frac{\sqrt[3]{3330}}{42} \approx 0.3555 \qquad (48)$$

$$l_p = \sqrt[3]{\frac{27783c^2 - 370\pi^2}{8232\pi^2}} \approx 0.8560 \qquad (49)$$

as compared to Eqs. (44) and (45).

Alternatively, the fourth order polynomial approximation to $f'(\eta)$

$$f_w'(\eta) = c\eta + (4 - 3c)\eta^3 + (2c - 3)\eta^4 \qquad (50)$$

may be used. The viscous boundary-layer thickness for this profile is given by

$$\delta_w^2 = \frac{420cx^3}{72 + 39c - 19c^2} \qquad (51)$$

and

$$x_{0_w} = \sqrt[3]{\frac{5(72 + 39c - 19c^2)}{21c(8 + 3c)^2}} \approx 0.46697 \qquad (52)$$

$$l_w = \sqrt[3]{\frac{567c^3(8 + 3c)^2 - 40\pi^2(72 + 39c - 19c^2)}{168\pi^2 c(8 + 3c)^2}} \approx 0.8293 \qquad (53)$$

which very closely approximate Eqs. (44) and (45). Consequently, the polynomial $f_w'(\eta)$ is used in subsequent developments of velocity and temperature distributions.

The temperature characteristics of Region 1 are now considered. The energy integral equation of Eq. (19) becomes

$$\left(\frac{1}{x^2}\right)\frac{d}{dx}\int_0^{\delta_T(x)} \bar{U}(1 - \bar{\phi})d\bar{Y} = \frac{1}{\text{Pr}}\left(\frac{\partial\bar{\phi}}{\partial\bar{Y}}\right)_{\bar{Y}=0} \qquad (54)$$

where $\delta_T(x)$ denotes the outer limits of the region of thermal diffusion. When $\text{Pr} > 1$, it may be anticipated that $\delta_T(x) < \delta(x)$ over $0 < x < x_0$. With $\eta_T = \bar{Y}/\delta_T(x)$ and the ratio δ_T/δ denoted by Δ so that $\eta = \Delta\eta_T$, the solution for $\delta_T(x)$ may be developed by assuming profiles for $\bar{U}$ and $\bar{\phi}$.

The two profile pairs of Ref. [4] have been used

$$\bar{U}(\eta) = f_p'(\eta), \quad \bar{\phi}(\eta_T) = f_p'(\eta_T)$$

$$\bar{U}(\eta) = f_w'(\eta), \quad \bar{\phi}(\eta_T) = f_w'(\eta_T) \qquad (55)$$

as each pairing ensures identical velocity and temperature distributions for $\text{Pr} = 1$ when also $\Delta = 1$. It is expected that the second pairing has advantages in effecting the transition at the end of Region 1.

The resultant equations for Δ are

$$\Delta^3(168 - 27\Delta^2 + 7\Delta^3) = \frac{148}{\text{Pr}} \qquad (56)$$

$$\Delta^2 D(\Delta) = \frac{4(72 + 39c - 19c^2)}{\text{Pr}} \qquad (57)$$

where $D(\Delta) = 168c(3 - c)\Delta + 27(4 - 3c)(5 - 2c)\Delta^3 - 7(3 - 2c)(12 - 5c)\Delta^4$, as obtained previously.

5.3 Region 2. The continuing diffusion of hot wall effects within a hydrodynamic setting prescribed by the Watson similarity solution is monitored in Region 2. The velocity on the free surface is no longer uniform but is prescribed in nondimensional terms by Eq. (29). The viscous boundary-layer thickness $\delta(x)$ is now one and the same as $\bar{h}(x)$, namely,

$$\delta(x) = \bar{h}(x) = \frac{2\pi}{3\sqrt{3}}(x^3 + l_w^3)$$

The energy integral equation (Eq. (54)) remains appropriate, and the progressive thermal diffusion implies that $\delta_T(x) \to \delta(x) = \bar{h}(x)$. In prescribing profiles, $\eta_T = \bar{Y}/\delta_T(x)$ may again be utilized, but now $\Delta(x) = \delta_T(x)/\delta(x)$ is no longer constant and tends to 1 at the end of Region 2.

An equation for $\delta_T(x)$ may be obtained by introducing the following profiles into the energy equation

$$\bar{U}(x, \eta) = \bar{U}_s(x)f_w'(\eta)$$

$$\bar{\phi}(x, \eta_T) = f_w'(\eta_T) \qquad (58)$$

to give

$$\frac{\delta_T(x)}{x^2}\frac{d}{dx}[\bar{U}_s(x)D(\Delta)\delta_T(x)] = \frac{2520c}{\text{Pr}} \qquad (59)$$

which in turn leads to

$$\frac{d}{dx}(\Delta^2) = \frac{10080x^2}{c\text{Pr}(x^3 + l_w^3)\Delta[336c(3 - c) + 108(4 - 3c)(5 - 2c)\Delta^2 - 35(3 - 2c)(12 - 5c)\Delta^3]} \qquad (60)$$

This first order equation may now be integrated with initial data $\Delta(x_{0w}; \text{Pr})$ as far as $\Delta(x_{1w}(\text{Pr}); \text{Pr}) = 1$.

$$\Delta^3[3360c(3 - c) + 648(4 - 3c)(5 - 2c)\Delta^2 - 175(3 - 2c)(12 - 5c)\Delta^3]$$

$$= \frac{50400}{c\text{Pr}}\ln\frac{x^3 + l_w^3}{x_{1w}^3 + l_w^3} + 6660 + 2001c - 1222c^2 \qquad (61)$$

where x_{1w} is used to denote the end of Region 2, as predicted using the Watson polynomial profile. Beyond x_{1w}, viscous and thermal effects are present throughout the film. For comparison, the Pohlhausen equivalent has also been computed and included

in the subsequent illustration of results.

The values of $x_{1w}(\text{Pr})$ are listed in Table 1. The numerical details for various Pr are presented in Table 2.

5.4 Region 3. In both Regions 1 and 2, it has been assumed that at the edge of the developing thermal boundary layer the temperature smoothly assimilates into that of the impinging jet. As a consequence, zero heat flux has been invoked. In Region 3, the same boundary condition, in fact, remains valid. Here, however, it is justified by the assumption of negligible heat transfer between the liquid free surface and the surrounding air. Consequently, the temperature of the film rises as a result of continuing heat input at

Table 1 The values of x_{1w} (Pr) for various Prandtl numbers

Pr	x_{1w} (Pr)
1.0	0.4670
2.0	0.6274
3.0	0.7513
4.0	0.8616
5.0	0.9663
6.0	1.0691
7.0	1.1722
8.0	1.2773
9.0	1.3856
10.0	1.4980

(a)

(b)

Fig. 2 (*a*) Comparison of free surface velocity for the respective profiles; (*b*) free surface velocity for the numerical solution and the present profile

the plate. The temperature is thus asymptotic to T_w.

Using the following profiles:

$$\bar{U}(x,\eta) = \bar{U}_s(x) f'_w(\eta)$$

$$\bar{\phi}(x,\eta) = \beta(x) f'_w(\eta) \tag{62}$$

where now $\eta = \bar{Y}/\bar{h}(x)$, the energy integral equation now reads

$$\left(\frac{1}{x^2}\right)\left[\frac{d}{dx}\int_0^{\bar{h}(x)} \bar{U}(\beta-\bar{\phi})d\bar{Y} - \int_0^{\bar{h}(x)} \bar{U}\frac{d\beta}{dx}d\bar{Y}\right] = \frac{1}{\text{Pr}}\left(\frac{\partial\bar{\phi}}{\partial\bar{Y}}\right)_{\bar{Y}=0} \tag{63}$$

Here, $\beta(x)$ monitors the adjustment of the film temperature to T_w. The result is an equation for $\beta(x)$ within the framework of the prescribed film thickness, namely,

$$\frac{72+39c-19c^2}{630}\frac{d}{dx}[\bar{U}_s\bar{h}\beta] - \frac{8+3c}{20}\bar{U}_s\bar{h}\frac{d\beta}{dx} = \frac{c}{\text{Pr}}\frac{\beta x^2}{\bar{h}} \tag{64}$$

Remembering that $\bar{U}_s(x)\bar{h}(x) = 3\sqrt{3}c^2/4\pi$, Eq. (64) becomes

$$\frac{d\beta}{dx} = -\frac{2520\beta x^2}{c(360+111c+38c^2)\text{Pr}(x^3+l_w^3)} \tag{65}$$

and, hence,

$$\beta(x) = \left(\frac{x_{1w}^3+l_w^3}{x^3+l_w^3}\right)^{840/c(360+11c+38c^2)\text{Pr}} \approx \left(\frac{x_{1w}^3+l_w^3}{x^3+l_w^3}\right)^{1.015/\text{Pr}} \tag{66}$$
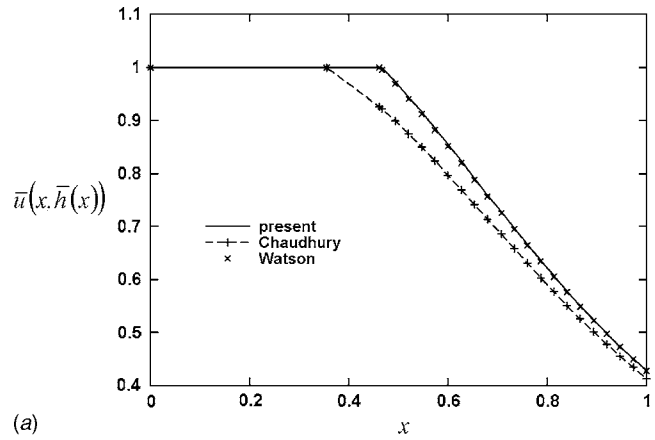
which satisfies the requirements $\beta[x_{1w}(\text{Pr})] = 1$ and has $\beta \to 0$ at rates dependent on Pr.
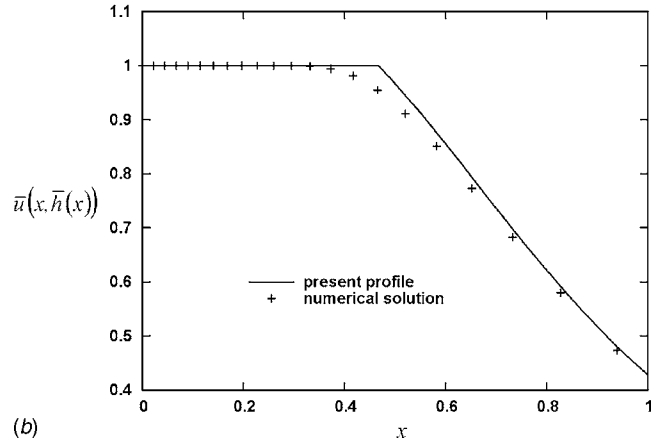
6 Approximation Results

The approximation scheme outlined provides comprehensive details of the flow and heat transfer characteristics for the model flow. Estimates of film thickness, velocity and temperature distri-

Table 2 Numerical results for $\Delta(x)$ in Region 2 for various Prandtl numbers

$\dfrac{x-x_{0w}}{x_{1w}-x_{0w}}$	$\Delta(x)$ Pr=2	Pr=5	Pr=10
0.0	0.7878	0.5775	0.4575
0.1	0.8092	0.6253	0.5347
0.2	0.8306	0.6728	0.6085
0.3	0.8520	0.7193	0.6769
0.4	0.8734	0.7644	0.7389
0.5	0.8947	0.8081	0.7948
0.6	0.9160	0.8500	0.8450
0.7	0.9372	0.8902	0.8899
0.8	0.9583	0.9286	0.9304
0.9	0.9792	0.9652	0.9669
1.0	1.0000	1.0000	1.0000

butions, skin friction, and heat transfer coefficients over the entire region downstream of the point of impingement can be obtained.

6.1 Film Thickness and Velocity and Temperature Distributions. To indicate the underlying implications of the hydrodynamic modeling, the free surface velocity has been illustrated for the respective profiles in Fig. 2(*a*). The associated velocity profile development within the deflected film is illustrated schematically in Fig. 3. Overall predictions of film thicknesses appear in Fig. 4(*a*). A more detailed indication of the region by region form of solution appears in Fig. 5. For the range of Prandtl numbers Pr=2, 5, and 10, film thickness profiles incorporating the viscous and thermal diffusion processes to penetration are presented. A typical set of temperature distributions within the film covering the evolution between initial thermal diffusion and the asymptotic linear profile is illustrated in Fig. 6.

6.2 Skin Friction and Heat Transfer Coefficients. The elements of interest in engineering practice are the shear stress at the solid boundary, i.e., the skin friction and the rate of heat transfer at the boundary. The skin friction is defined as

$$\tau = \mu\left(\frac{\partial v_r}{\partial z}\right)_{z=0} \tag{67}$$

leading to the nondimensional skin friction coefficient

$$\bar{\tau} = \left(\frac{H_0^2\mu^2}{\rho U_0^4}\right)^{1/3}\frac{\tau}{x} = \frac{\tau \text{Re}^{2/3}}{\rho U_0^2 x} = \left(\frac{\partial\bar{U}}{\partial\bar{Y}}\right)_{\bar{Y}=0} \tag{68}$$
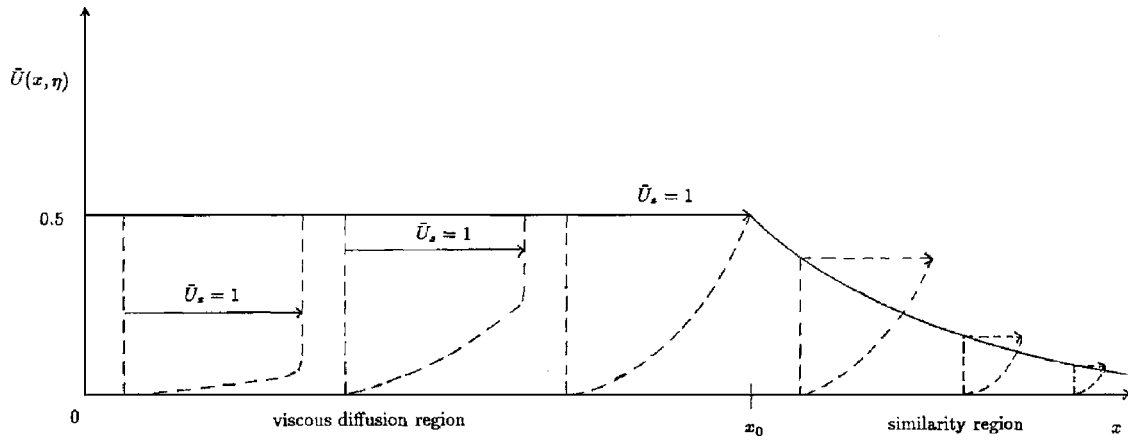
From the approximations, it gives

Fig. 3   Velocity profile development within the deflected film

$$\bar{\tau}_p = \sqrt{\frac{37}{105x^3}} \quad \text{(in Region 1)}$$

$$= \frac{81\sqrt{3}c^2}{8\pi^3(x^3 + l_p^3)^2} \quad \text{(in Regions 2 and 3)} \qquad (69)$$

$$\bar{\tau}_w = \sqrt{\frac{(72 + 39c - 19c^2)c}{420x^3}} \quad \text{(in Region 1)}$$

$$= \frac{81\sqrt{3}c^3}{16\pi^3(x^3 + l_w^3)^2} \quad \text{(in Regions 2 and 3)} \qquad (70)$$

Graphs of $\bar{\tau}(x)$ are plotted in Fig. 7(a). The integrable square root singularity is consistent with the Blasius boundary-layer equivalent.

The most significant film cooling design factor is the heat transfer across the film. The heat transfer at the solid boundary is given by

$$q = -\kappa\left(\frac{\partial T}{\partial z}\right)_{z=0} = \frac{\kappa\Delta T \mathrm{Re}^{1/3}x}{H_0}\left(\frac{\partial \bar{\phi}}{\partial \bar{Y}}\right)_{\bar{Y}=0} \qquad (71)$$

where $\Delta T = T_w - T_0$. The nondimensional version of this is known as the Nusselt number defined as

$$\mathrm{Nu} = \frac{qH_0}{\kappa\Delta T \mathrm{Re}^{1/3}x} = \left(\frac{\partial \bar{\phi}}{\partial \bar{Y}}\right)_{\bar{Y}=0} \qquad (72)$$

The results are

$$\mathrm{Nu}_p = \frac{1}{\Delta_p(\mathrm{Pr})}\sqrt{\frac{37}{105x^3}} \quad \text{(in Region 1)}$$

$$= \frac{1}{\Delta_p(x;\mathrm{Pr})}\frac{3\sqrt{3}}{\pi(x^3 + l_p^3)} \quad \text{(in Region 2)}$$

$$= \frac{3\sqrt{3}}{\pi(x^3 + l_p^3)}\left(\frac{x_{1_p}^3 + l_p^3}{x^3 + l_p^3}\right)^{840/367c^2\mathrm{Pr}} \quad \text{(in Region 3)} \qquad (73)$$
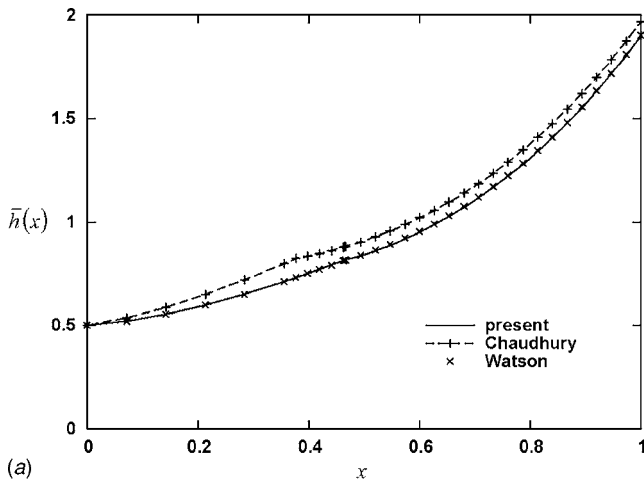
and

$$\mathrm{Nu}_w = \frac{1}{\Delta_w(\mathrm{Pr})}\sqrt{\frac{(72 + 39c - 19c^2)c}{420x^3}} \quad \text{(in Region 1)}$$
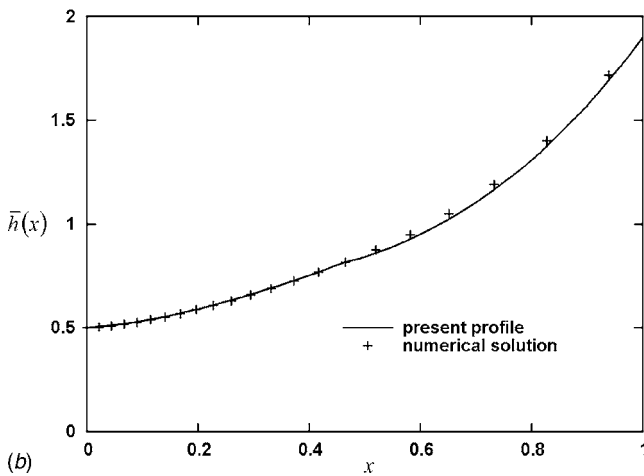
$$= \frac{1}{\Delta_w(x;\mathrm{Pr})}\frac{3\sqrt{3}c}{2\pi(x^3 + l_w^3)} \quad \text{(in Region 2)}$$

$$= \frac{3\sqrt{3}c}{2\pi(x^3 + l_w^3)}\left(\frac{x_{1_w}^3 + l_w^3}{x^3 + l_w^3}\right)^{840/c(360+111c+38c^2)\mathrm{Pr}} \quad \text{(in Region 3)}$$

$$(74)$$

The predictions of Nu_w for a range of Prandtl numbers are presented in Fig. 8(a). The values of $\Delta_p(\mathrm{Pr})$ and $\Delta_w(\mathrm{Pr})$ have been obtained from Eqs. (56) and (57), respectively. $\Delta_w(x;\mathrm{Pr})$ satisfies

(a)

(b)

Fig. 4   (a) Comparison of film thickness for the respective profiles; (b) film thickness for the numerical solution and the present profile
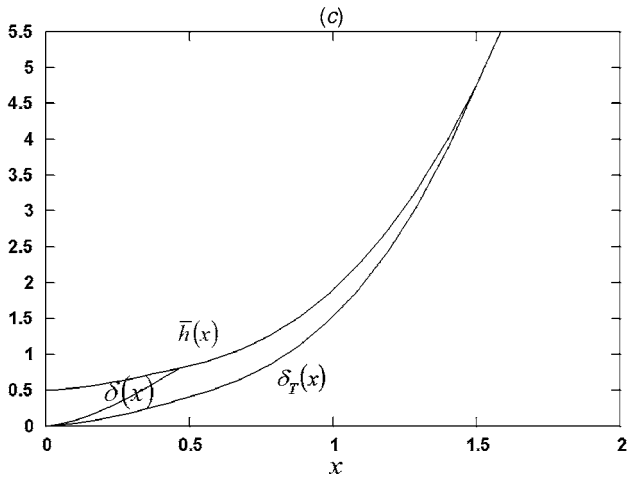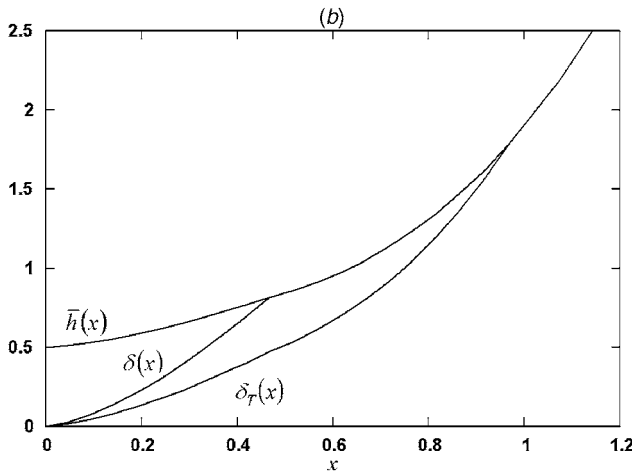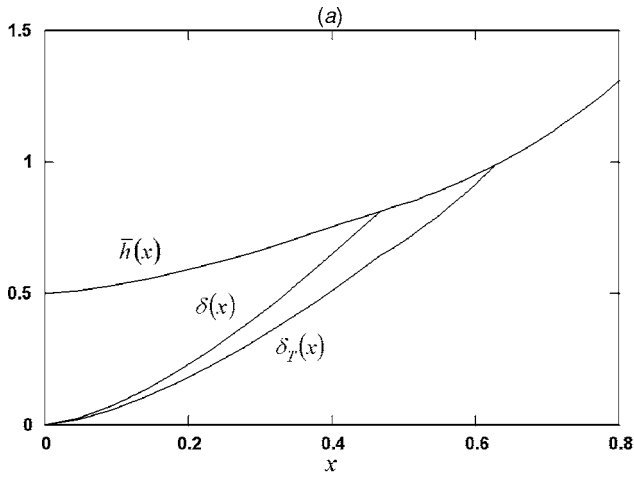
Fig. 5 Film, viscous, and thermal boundary-layer thicknesses for Pr=(a) 2, (b) 5, and (c) 10 using the present profile

Eq. (61). Accordingly, $\Delta_p(x;\mathrm{Pr})$ satisfies the following equation:

$$\Delta^3(3360 - 648\Delta^2 + 175\Delta^3) = \frac{50,400}{c^2\mathrm{Pr}} \ln \frac{x^3 + l_p^3}{x_{1_p}^3 + l_p^3} + 2887 \quad (75)$$

7 Numerical Solutions

The continuity (Eq. (10)) is eliminated by introducing a stream function ψ defined by

$$\bar{U} = \frac{1}{x}\frac{\partial \psi}{\partial \bar{Y}}, \quad \bar{V} = -\frac{1}{x}\frac{\partial \psi}{\partial x} \quad (76)$$

Owing to the geometry, $\bar{H}(x)$ is singular at $x=0$. To remove this singularity, y and $\bar{h}(x)$ are introduced and given by

$$y = x\bar{Y}, \quad \bar{h}(x) = x\bar{H}(x) \quad (77)$$

Substituting Eqs. (76) and (77) into Eqs. (10)–(16) gives

$$\frac{\partial^3 \psi}{\partial y^3} = \left(\frac{1}{x^2}\right)\left(\frac{\partial \psi}{\partial y}\frac{\partial^2 \psi}{\partial x \partial y} - \frac{\partial \psi}{\partial x}\frac{\partial^2 \psi}{\partial y^2}\right) \quad (78)$$

$$\frac{\partial^2 \bar{\phi}}{\partial y^2} = \left(\frac{\mathrm{Pr}}{x^2}\right)\left(\frac{\partial \psi}{\partial y}\frac{\partial \bar{\phi}}{\partial x} - \frac{\partial \psi}{\partial x}\frac{\partial \bar{\phi}}{\partial y}\right) \quad (79)$$

subject to boundary conditions

$$\psi = 0, \quad \frac{\partial \psi}{\partial y} = 0, \quad \bar{\phi} = 0 \quad \text{at } y = 0, \ x \geq 0 \quad (80)$$

$$\psi = \frac{1}{2}, \quad \frac{\partial^2 \psi}{\partial y^2} = 0, \quad \frac{\partial \bar{\phi}}{\partial y} = 0 \quad \text{at } y = \bar{h}(x), \ x \geq 0 \quad (81)$$

$$\bar{h} = \frac{1}{2}, \quad \psi = y, \quad \bar{\phi} = 1 \quad \text{at } x = 0, \ 0 < y \leq \frac{1}{2} \quad (82)$$

where the initial condition (Eq. (82)) appears due to the original initial condition

$$H = \frac{H_0^2}{2r}, \quad v_r = U_0, \quad T = T_0 \quad \text{at } r = 0, \ 0 < z \leq \frac{H_0^2}{2r} \quad (83)$$

In anticipation of the use of a Keller box method and its attractive extrapolation features, the differential system (Eqs. (78)–(82)) is recast as the following first order system:

$$\frac{\partial \psi}{\partial y} = \bar{u}$$

$$\frac{\partial \bar{u}}{\partial y} = \bar{v}$$

$$\frac{\partial \bar{v}}{\partial y} = \left(\frac{1}{x^2}\right)\left(\bar{u}\frac{\partial \bar{u}}{\partial x} - \bar{v}\frac{\partial \psi}{\partial x}\right)$$

$$\frac{\partial \bar{\phi}}{\partial y} = \bar{w}$$

$$\frac{\partial \bar{w}}{\partial y} = \left(\frac{\mathrm{Pr}}{x^2}\right)\left(\bar{u}\frac{\partial \bar{\phi}}{\partial x} - \bar{w}\frac{\partial \psi}{\partial x}\right) \quad (84)$$

whose boundary conditions are

$$\psi = 0, \quad \bar{u} = 0, \quad \bar{\phi} = 0 \quad \text{at } y = 0, \ x \geq 0$$

$$\psi = \frac{1}{2}, \quad \bar{v} = 0, \quad \bar{w} = 0 \quad \text{at } y = \bar{h}(x), \ x \geq 0$$

$$\bar{h} = \frac{1}{2}, \quad \psi = y, \quad \bar{\phi} = 1 \quad \text{at } x = 0, \ 0 < y \leq \frac{1}{2} \quad (85)$$

The following coordinate transformation, what simultaneously maps the film thickness onto the unit interval and removes the Blasius singularity at the origin, is introduced

$$x = \xi^{2/3}, \quad y = \frac{\xi \eta \bar{h}}{\xi + 1 - \eta}$$

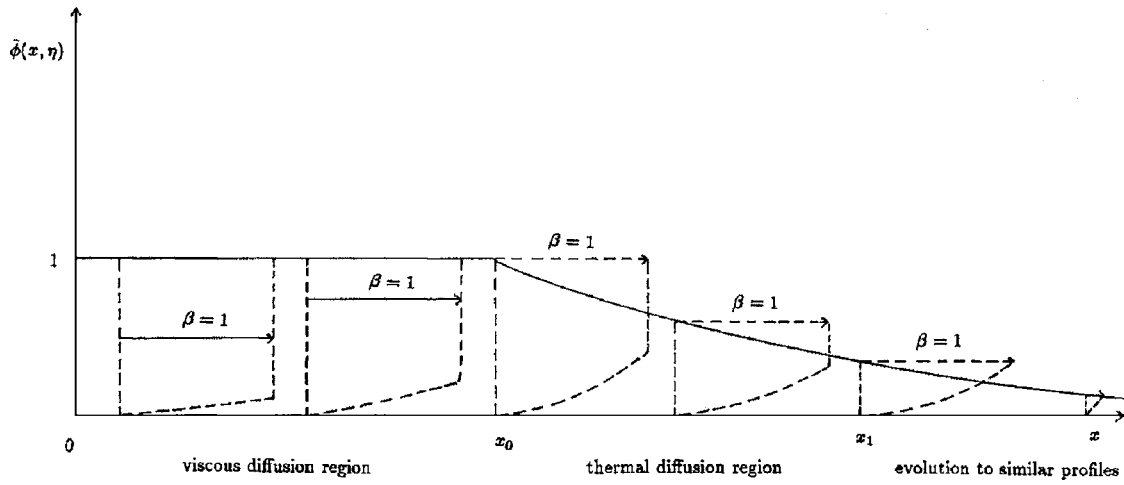The dependent variables are transformed as

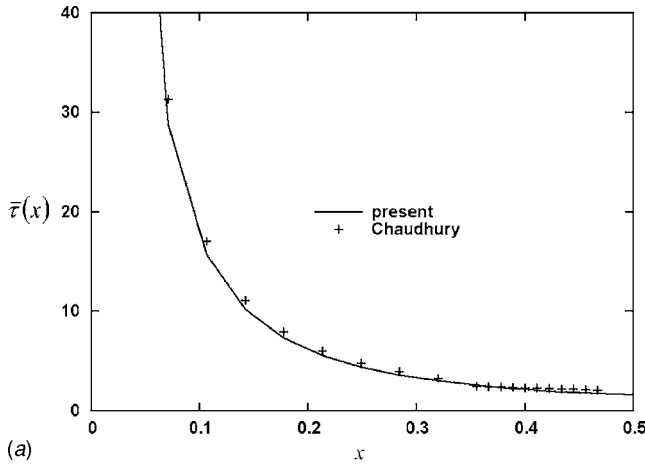**Fig. 6 Temperature profile development within the deflected film**

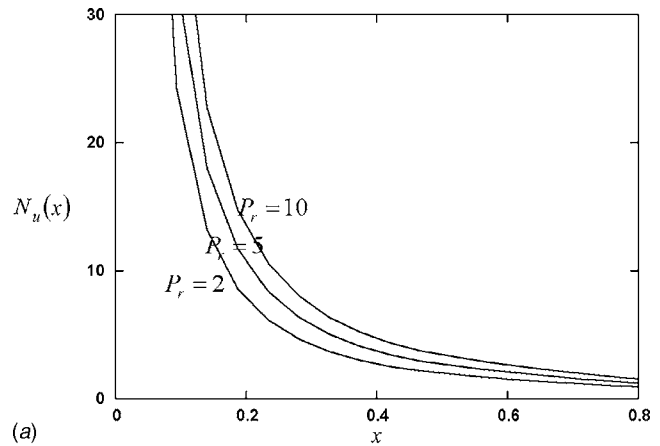$$\psi = \frac{\xi}{\xi + 1 - \eta} f, \quad \bar{u} = \frac{u}{(1 + \xi)^2}, \quad \bar{v} = \frac{\xi + 1 - \eta}{\xi(1 + \xi)^4} v$$

$$\bar{\phi} = \phi, \quad \bar{w} = \frac{\xi + 1 - \eta}{\xi(1 + \xi)^2} w, \quad \bar{h} = (1 + \xi)^2 h$$

The equations to be solved now read

$$f_\eta = \frac{(1 + \xi)hu}{\xi + 1 - \eta} - \frac{f}{\xi + 1 - \eta}$$

$$u_\eta = \frac{(1 + \xi)hv}{\xi + 1 - \eta}$$
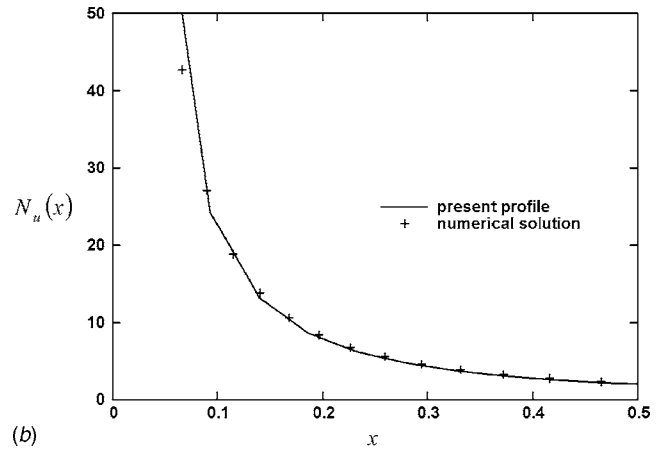

(a)
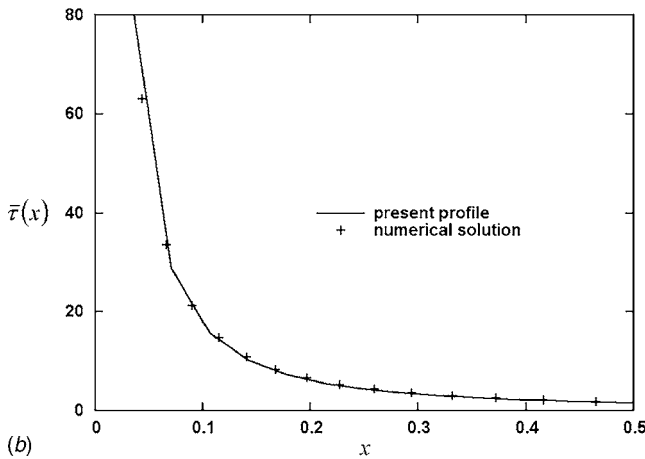
(b)

Fig. 7 (*a*) **Skin friction for the present and the Chaudhury profiles;** (*b*) **skin friction for the numerical solution and the present profile**

(a)

(b)

Fig. 8 (*a*) **Heat transfer coefficient for various Prandtl numbers;** (*b*) **heat transfer coefficient for the numerical solution and the present profile at Pr=2**

Journal of Heat Transfer

$$v_\eta = \frac{v}{\xi+1-\eta} - \frac{3\xi(1+\xi)^2 hu^2}{(\xi+1-\eta)^3} - \frac{3(1-\eta)(1+\xi)^3 hfv}{2(\xi+1-\eta)^4}$$
$$+ \frac{3\xi(1+\xi)^3 h}{2(\xi+1-\eta)^3}(uu_\xi - vf_\xi)$$

$$\phi_\eta = \frac{(1+\xi)hw}{\xi+1-\eta}$$

$$w_\eta = \frac{w}{\xi+1-\eta} - \frac{3\text{Pr}(1-\eta)(1+\xi)^3 hfw}{2(\xi+1-\eta)^4}$$
$$+ \frac{3\text{Pr}\xi(1+\xi)^3 h}{2(\xi+1-\eta)^3}(u\phi_\xi - wf_\xi) \qquad (86)$$

subject to

$$f=0, \quad u=0, \quad \phi=0 \quad \text{at } \eta=0, \ \xi \geqslant 0$$

$$f=\frac{1}{2}, \quad v=0, \quad w=0 \quad \text{at } \eta=1, \ \xi \geqslant 0$$

$$h=\frac{1}{2}, \quad f=f_0(\eta), \quad \phi=\phi_0(\eta) \quad \text{at } \xi=0, \ 0<\eta \leqslant 1 \quad (87)$$

where the initial profiles $f_0(\eta)$ and $\phi_0(\eta)$ are found by putting ξ $=0$ and $h=1/2$ into Eq. (86) and solving, subject to conditions $f=u=\phi=0$ at $\eta=0$ and $u=1$, $\phi=1$ at $\eta=1$.

The parabolic system of equations and boundary conditions (Eqs. (86) and (87)) has been solved by marching in the ξ direction using a modification of the Keller box method. A nonuniform grid is placed on the domain $\xi \geqslant 0$, $0 \leqslant \eta \leqslant 1$, and the resulting difference equations are solved by Newton iteration. Solutions are obtained on different sized grids and Richardson's extrapolation used to produce results of high accuracy. A full account of the numerical method and the details of implementation are beyond the scope of this paper and will be reported separately [13]. The detailed numerical method procedure for this case is fully discussed in Ref. [1]. For the axisymmetric flat plate in this paper, the relevant physical parameters should be chosen as

$$F(x)=0 \quad G(x)=\frac{1}{x} \quad x_s=+\infty \quad \gamma=\frac{1}{2} \quad \alpha=\frac{2}{3} \quad \beta=2$$

The solution scheme was successfully tested against previously reported results [14–19].

8 Results

A typical run has a coarse grid of dimension 60×48 in the (ξ, η) domain with each cell being divided into one to four subcells. Because of the coordinate singularity at $\xi=0$, $\eta=1$, a nonuniform grid is employed and given by $\xi=(1/3)\sinh[\bar{\xi}^{1.5}(1+\bar{\xi}^{1.5})]$, $\eta=1-(1-\bar{\eta})^{1.5}$, where $\bar{\xi}$ and $\bar{\eta}$ are uniform. When $\Delta\bar{\xi} \equiv 0.044618955$ and $\Delta\bar{\eta} \equiv 1/47$, this gives $\Delta\xi \sim 0.004$ and $\Delta\eta \sim 0.003$ near the singularity, which is sufficiently small to give good accuracy, and this enabled us to integrate as far as $\xi \sim 10^9$, which is necessary for the profile at infinity to be determined with sufficient accuracy. From the convergence of the extrapolation process, the absolute error is 9×10^{-7}. A typical set of numerical data is presented in Table 3.

Figures 2(b), 4(b), 7(b), 8(b), and 9(a) show excellent agreement between the full numerical solutions and the theoretical results obtained using an assumed present quartic velocity profile (Eq. (50)). Figure 9(b) shows free surface temperature for various Prandtl numbers. As Pr increases, the temperature decrease becomes more gradual.

Table 3 Film thickness, free surface velocity, and temperature for the axisymmetric flat plate with Pr=2

x	Film thickness $\bar{h}(x)$	Free surface velocity $\bar{u}[x,\bar{h}(x)]$	Free surface temperature $\bar{\phi}[x,\bar{h}(x)]$
0.000	0.500	1.000	1.000
0.115	0.539	1.000	1.000
0.197	0.587	1.000	1.000
0.294	0.659	1.000	1.000
0.416	0.767	0.981	0.999
0.520	0.875	0.911	0.989
0.733	1.191	0.682	0.891
1.072	2.206	0.368	0.660
1.669	6.338	0.128	0.389
1.968	9.930	8.188×10^{-2}	0.310
2.817	27.742	2.931×10^{-2}	0.185
5.228	1.735×10^2	4.685×10^{-3}	7.372×10^{-2}
10.791	1.520×10^3	5.348×10^{-4}	2.484×10^{-2}
25.010	1.892×10^4	4.297×10^{-5}	7.031×10^{-3}
46.931	1.250×10^5	6.504×10^{-6}	2.734×10^{-3}
1.347×10^2	2.957×10^6	2.749×10^{-7}	5.620×10^{-4}
1.073×10^3	1.495×10^9	5.438×10^{-10}	2.500×10^{-5}
1.321×10^4	2.784×10^{12}	2.920×10^{-13}	6.00×10^{-7}
1.385×10^5	3.212×10^{15}	2.531×10^{-16}	0.000
1.000×10^6	1.209×10^{18}	6.723×10^{-19}	0.000

9 Concluding Remarks

Both numerical and approximate solutions for the flow of a cold axisymmetric vertical jet against a horizontal flat plate have been obtained. The level of agreement in estimating film thickness and velocity and temperature distributions is remarkably good insofar
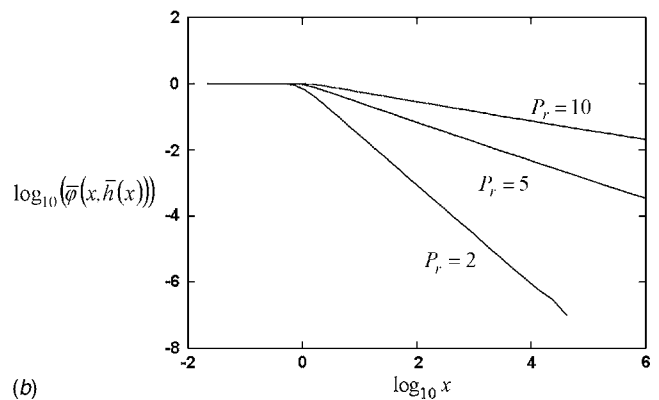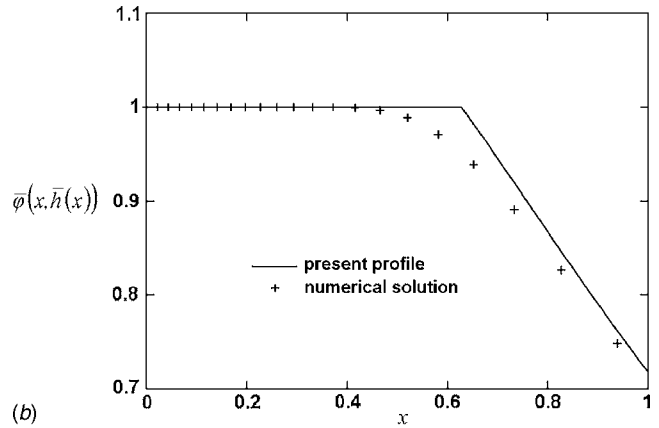

Fig. 9 (a) Free surface temperature for the numerical solution and the present profile at Pr=2 (b) free surface temperature for various Prandtl numbers

as predictions of skin friction and heat transfer characteristics are concerned. Although it is valuable to have demonstrated a successful, robust Keller-box algorithm, it is also noteworthy that the approximation may provide a satisfactory methodology for the assessment of practical configurations, sufficient for the purposes of engineering practice.

Nomenclature

C_p = specific heat
(f, u, v, ϕ, w) = dependent variables
f_0, ϕ_0 = initial profiles
H, h = film thicknesses
H_0 = jet semithickness
k = thermal conductivity
l = leading edge shift constant
Nu = Nusselt number
P, p = pressure
Pr = Prandtl number
Q = $U_0 H_0$
q = heat flux
$(r, z), (x, Y)$ = Cartesian coordinates measured along and normal to the plate
Re = Reynolds number
T = temperature
T_0 = jet temperature
T_w = plate temperature
U_0 = jet velocity
$\bar{U}_s$ = free surface velocity
$\mathbf{V} = (U, V)$ = velocity and its components
x_0, x_1 = ends of Regions 1 and 2

Greek Symbols

β = dimensionless free surface temperature
Γ = gamma function
Δ = δ_T / δ
δ, δ_T = dimensionless boundary-layer thicknesses of velocity and temperature variations
η_T = η / Δ
κ = thermometric conductivity
μ, ν = dynamic and kinematic viscosities
(ξ, η) = dimensionless coordinates
ρ = density
τ = skin friction
ψ = stream function

Subscript

w = Watson

Superscript

$\bar{}$ = dimensional analysis

References

[1] Shu, J.-J., and Wilks, G., 2007, "Heat Transfer in the Flow of a Cold, Two-Dimensional Draining Sheet Over a Hot, Horizontal Cylinder," Eur. J. Mech. B/Fluids, **26**(6), pp. 1–5.
[2] Watson, E. J., 1964, "The Radial Spread of a Liquid Jet Over a Horizontal Plane," J. Fluid Mech., **20**(3), pp. 481–499.
[3] Chaudhury, Z. H., 1964, "Heat Transfer in a Radial Liquid Jet," J. Fluid Mech., **20**(3), pp. 501–511.
[4] Shu, J.-J., and Wilks, G., 1996, "Heat Transfer in the Flow of a Cold, Two-Dimensional Vertical Liquid Jet Against a Hot, Horizontal Plate," Int. J. Heat Mass Transfer, **39**(16), pp. 3367–3379.
[5] Zhao, Y. H., Masuoka, T., Tsuruta, T., and Ma, C. F., 2002, "Conjugated Heat Transfer on a Horizontal Surface Impinged by Circular Free-Surface Liquid Jet," JSME Int. J., Ser. B, **45**(2), pp. 307–314.
[6] Shu, J.-J., 2004, "Microscale Heat Transfer in a Free Jet Against a Plane Surface," Superlattices Microstruct., **35**(3–6), pp. 645–656.
[7] Guerra, D. R. S., Su, J., and Freire, A. P. S., 2005, "The Near Wall Behavior of an Impinging Jet," Int. J. Heat Mass Transfer, **48**(14), pp. 2829–2840.
[8] Rice, J., Faghri, A., and Cetegen, B., 2005, "Analysis of a Free Surface Film From a Controlled Liquid Impinging Jet Over a Rotating Disk Including Conjugate Effects, With and Without Evaporation," Int. J. Heat Mass Transfer, **48**(25–26), pp. 5192–5204.
[9] Shu, J.-J., and Wilks, G., 2007, "Heat Transfer in the Flow of a Cold, Axisymmetric Jet Over a Hot Sphere," Int. J. Therm. Sci., **46**(12), pp. 1–5.
[10] Shu, J.-J., 2004, "Impact of an Oblique Breaking Wave on a Wall," Phys. Fluids, **16**(3), pp. 610–614.
[11] Shu, J.-J., 2004, "Slamming of a Breaking Wave on a Wall," Phys. Rev. E, **70**(6), p. 066306.
[12] Rosenhead, L., 1963, *Laminar Boundary Layers*, Oxford University Press, New York.
[13] Shu, J.-J., and Wilks, G., 1995, "An Accurate Numerical Method for Systems of Differentio-Integral Equations Associated With Multiphase Flow," Comput. Fluids, **24**(6), pp. 625–652.
[14] Shu, J.-J., and Wilks, G., 1995, "Mixed-Convection Laminar Film Condensation on a Semi-Infinite Vertical Plate," J. Fluid Mech., **300**, pp. 207–229.
[15] Shu, J.-J., and Pop, I., 1997, "Inclined Wall Plumes in Porous Media," Fluid Dyn. Res., **21**(4), pp. 303–317.
[16] Shu, J.-J., and Pop, I., 1998, "Transient Conjugate Free Convection from a Vertical Flat Plate in a Porous Medium Subjected to a Sudden Change in Surface Heat Flux," Int. J. Eng. Sci., **36**(2), pp. 207–214.
[17] Shu, J.-J., and Pop, I., 1998, "On Thermal Boundary Layers on a Flat Plate Subjected to a Variable Heat Flux," Int. J. Heat Fluid Flow, **19**(1), pp. 79–84.
[18] Shu, J.-J., and Pop, I., 1999, "Thermal Interaction Between Free Convection and Forced Convection Along a Conducting Plate Embedded in a Porous Medium," Hybrid Methods in Engineering: ---Modeling, Programming, Analysis, Animation, **1**(1), pp. 55–66.
[19] Shu, J.-J., and Pop, I., 1999, "Thermal Interaction Between Free Convection and Forced Convection Along a Vertical Conducting Wall," Heat Mass Transfer, **35**(1), pp. 33–38.